Stationary Planetary Waves Inferred from WINDII Wind Data Taken within Altitudes 90–120 km during 1991–96

D. Y. WANG, W. E. WARD, AND G. G. SHEPHERD

Centre for Research in Earth and Space Technology, York University, North York, Ontario, Canada

DONGS-LIANG WU

Jet Propulsion Lab, California Institute of Technology, Pasadena, California

(Manuscript received 22 May 1998, in final form 22 July 1999)

ABSTRACT

A climatology of stationary planetary waves (SPWs) in horizontal winds at latitudes 70°S–70°N and altitudes 90–120 km is obtained from Wind-Imaging Interferometer (WINDII) green line measurements in December–January and March–April of 1991–96. The observed solstitial SPW fields are relatively stronger and dominated by zonal wavenumber-1 variations. In contrast, the equinoctial SPW fields are weaker and characterized by zonal wavenumber-2 variations. The zonal amplitude maxima of 10–25 m s^{-1} are generally centered at the midlatitudes of 35°–40° in both hemispheres around 96 km, with the eastward perturbation velocity maxima around 90°E for wavenumber 1 and 60° and 240°E for wavenumber 2. The meridional amplitude maxima are about 5–15 m s^{-1} and show more variabilities in their latitude–height distributions. The meridional phases indicated that Eliassen–Palm (EP) fluxes were downward–poleward for the winter maxima, vertically varying poleward for the summer maxima, and more variable during March–April. The hemispheric–seasonal–interannual variations in amplitude and phase are of 10 m s^{-1} and 30°, respectively. In particular, a distinguishable local summer maximum with an amplitude of 10–20 m s^{-1} is found to exist in the wavenumber-1 variation of zonal wind component. The hemispheric asymmetry is also characterized by the nodal phase (or phase jump) lines shifted toward the winter hemisphere by 10°–30°. Wave penetrations across the equator are observed with amplitudes of 5 m s^{-1} at 97–100 km. While the summer maximum of the wavenumber-1 component persisted during the four years, large variability is found in the winter hemisphere where the wavenumber-2 component became significant at the 90–105-km region during December 1992–January 1993 and December 1993–January 1994 and at the 105–120-km region during December 1991–January 1992. The excitation due to in situ forcing of azonal gravity wave drag, which varies longitudinally, is thought to be largely responsible for the observed SPW, particularly for the summer maximum, while the leakage of upward propagating SPW from the lower to the higher atmosphere also plays a role, especially in the winter and the equinoctial periods.

1. Introduction

While there exists a number of studies on stationary planet waves (SPWs) in the stratosphere and mesosphere (for reviews, see Barnett and Labitzke 1990; Andrews et al. 1987), to date, their presence in the 90–120-km region of the mesosphere and lower thermosphere (MLT) for the most part has not been explored. The investigations of planetary waves in the region focus mostly on traveling modes, in particular, the two-day wave. This is because researchers interpreting disturbance measurements from a single ground station or a limited network of stations must assume that the features are traveling disturbances.

Corresponding author address: Dr. Ding-Yi Wang, Petrie 206, York University, 4700 Keele St., North York, ON M3J 1P3, Canada. E-mail: Ding@windop.yorku.ca

Because of the lack of relevant data, SPW variations between 90 and 130 km are not included in the current horizontal wind model (HWM-93) (Hedin et al. 1996). Theoretical investigations of SPW, however, have been carried out. Schoeberl and Geller (1977) provide an analysis of these waves extending to 100 km. Simulations of Medvedev et al. (1991) and Pogoreltsev and Sukhanova (1993) have revealed SPW perturbations with zonal amplitudes of 20 m s^{-1} at midlatitudes and 10 m s^{-1} at the equator in this height region. The SPW-induced mean zonal flow accelerations are comparable with those associated with gravity waves and atmospheric tides (Pogoreltsev 1996). McLandress and McFarlane (1993) and McLandress and Ward (1994) have shown that the interaction between the mean–tidal wind fields and the localized orographic gravity wave momentum flux can generate planetary-scale disturbances. Only recently have observations of SPW been reported. Smith (1996, 1997) (S96 and S97, hereafter)

presented some SPW observations using high resolution Doppler imager (HRDI) data between 50 and 100 km during northern winter (February and mid-March) and southern winter (August and September) for 1992–94, and suggested that in situ forcing of planetary-scale disturbances due to variations in gravity wave drag caused by stratospheric filtering was important.

The Wind-Imaging Interferometer (WINDII) experiment on board the *Upper Atmosphere Research Satellite* (*UARS*) has produced a unique global dataset, substantially increasing the quantity and quality of available wind measurements in the MLT region. This report uses WINDII data taken during December 1991–January 1996 to describe the climatology of SPW between 90 and 120 km. The mean features and the geographic and temporal variabilities in the SPW amplitudes and phases are analyzed. The data characteristics and our analysis method are briefly described in section 2. The inferred global SPW distributions for zonal wavenumbers 1 and 2 (wave 1 and 2) at solstice and equinox conditions are presented in section 3. Our conclusions are contained in section 4.

2. Data description and analysis

The wind data used for this study are derived from $O(^1S)$ airglow emissions observed by WINDII during 1991–96 and are calculated using V4.98 of the WINDII data analysis software. The observations cover an altitude region from 80 to 300 km in daytime and from 80 to 110 km in nighttime. For this study, however, data between 90 and 120 km are used. The latitudinal coverage of the data alternates from 72°S–40°N to 42°S–72°N throughout the course of a year, determined by the satellite pointing direction with a yaw period of 36 days. The vertical resolution of the data is 3 km below 120 km and 5 km at the upper heights. The WINDII dataset includes calculated errors. For the data used in this study, a threshold value of 7 m s^{-1} for the wind error and a signal-to-noise ratio (S/N) of 5 for the airglow emission intensity were chosen to exclude questionable wind velocities. Some wind measurements with apparently spurious values, probably due to auroral contamination, were also rejected. The number of available measurements for each day varies from the low tens to several hundreds. Data gaps may occur due to the selection criteria and/or observation interruption caused by frequent background calibration measurements and other airglow emission observations as well as power-off periods. A more detailed description of the experiment and the data characteristics can be found in Shepherd et al. (1993).

For planetary wave analysis, sampling around latitude circles provides a zonal cut through the wave. For stationary or slowly propagating waves, the observed wavenumber is that of the wave. As a result, the determination of SPW components in the horizontal winds begins with binning all longitudinal data at individual heights into latitude bins with a certain width (5° is used for this study). At a given latitude over the course of a day, about 30 longitudinal points are sampled, 15 in each of the ascending and descending nodes. The sampling in the two legs corresponds to two different local times, each of which remains approximately constant for successive orbits, changing by only 20 min per day. The daily means of available data points are computed separately for each leg. They represent the actual zonal mean winds and migrating tides and are subtracted from individual data points to effectively eliminate tidal influence on the residuals. The daily mean and residual datasets obtained from both legs are then combined to derive monthly mean winds and stationary waves, respectively. To further remove wind variations due to migrating/nonmigrating tides and traveling planetary wave components, two successive months of the datasets, in December–January and in March–April of each year, are combined to achieve a full 24 h of sampling.

The vector spherical expansion method described by Wang et al. (1997) is used to decompose the combined residual datasets into the SPW components of waves 1 and 2, and the daily means into the actual zonal mean winds and diurnal/semidiurnal tides. The atmospheric disturbances are described by a general form of

$$A_{\sigma s}(\theta, z)\cos[2\pi\sigma t + s\lambda + \alpha_{\sigma s}(\theta, z)], \qquad (1)$$

where t is universal time in day and λ is longitude in radians. The frequency and zonal wavenumber are σ and s, respectively. Their paired values, (σ, s), are used to denote a wave mode. For example, (0, 1), (0, 2), and (1, 1) indicate stationary wave 1, wave 2, and the migrating diurnal tide, respectively. The amplitude $A_{\sigma s}$ and phase $\alpha_{\sigma s}$ of each harmonic (σ, s) are assumed to be functions of latitude θ and altitude z.

In the above-described average and fitting processes, the individual measurements are weighted by their error estimates. In January 1995 and in March 1994, the data coverage was minimal, and hence, the derived mean winds and SPW components for the periods of December 1994–January 1995 and March–April 1994 are excluded from our discussion.

The asynoptic nature of the satellite sampling poses difficulties in the interpretation of the derived space–time spectra. At a given latitude–altitude grid point, the measurements covered by the ascending and descending nodes form a space–time series and are ordered asynoptically in longitude and coordinated universal time (UTC). The samples are not oriented in parallel to either the time or space axes. If they are ordered uniformly by some mean in time, they cannot be arranged uniformly in the space domain. As a result of the orbit tilt, both the longitude and time separations between ascending and descending traversals tend to zero as the poles are approached. This irregular character is tantamount to a latitudinal nonuniformity in the sampling pattern. The fundamental aliasing issues associated with these sampling features have been investigated by Salby

(1982a,b). The aliasing problems of WINDII data sampling are studied in a manner similar to that used by Wu et al. (1995) for the analysis of the 2-day wave observed by HRDI. To obtain all aliases of a given wave mode, we simply simulate a set of measurements in the presence of that wave alone and compute its periodogram (power spectrum) with the same sampling condition.

Figure 1 presents the simulated aliasing results for waves 1 and 2 at two latitude bins. The waves are taken as the artificial signal on WINDII sampling points during March–April 1992. Their power densities are normalized to units. All other components are their corresponding aliases. As expected from the aliasing mutuality, if one of these aliasing components were taken as the input signal, the same amount of aliasing would be correspondingly generated at wave 1 or 2. In Fig. 1, it is seen that the most serious aliases are associated with nonmigrating diurnal tides (1, 0) and (1, 2) for wave 1 and (1, −1) and (1, 3) for wave 2. The aliases from the nonmigrating diurnal tides are less than 20% at midlatitudes and low latitudes below 45° but can be as large as 40%–80% at high latitudes. The latitudinal variations of the aliases are shown in Fig. 2 for wave 1 and mode (2, 1) and for wave 2 and mode (1, −1). As shown in Fig. 1, the aliases of wave 1 and wave 2 with nonmigrating semidiurnal tides are not very important, about 20% at high latitudes and significantly reducing at midlatitudes and lower latitudes.

The simulation results can be used to justify our stationary wave analysis presented in the next section. The derived wave-1 and -2 fields at equinox (see section 3c) generally show zonal and meridional amplitudes of 5–10 m s^{-1} at the midlatitudes and low latitudes below 45°, where less than 20% aliasing may arise from nonmigrating diurnal and semidiurnal tidal components. At higher latitudes above 45°, the observed wave-1 and -2 amplitudes are negligibly small, although the aliases from the tidal components become significant. The same discussions can be readily extended to solstitial conditions for which the SPW and the tidal amplitudes are larger and smaller, respectively, in comparison with those at equinox. A 20% aliasing means that a 50–125 m s^{-1} amplitude of the nonmigrating tidal components is required to generate a 10–25 m s^{-1} amplitude of the commonly observed solstitial SPW at the midlatitudes and low latitudes. This probably allows one to rule out such a large nonmigrating tidal components in the observed SPW amplitudes.

3. Results and discussions

Latitude–height cross sections of the two-month mean zonal wind for December–January and March–April time periods are presented in Fig. 3. The meridional cross sections of the two-month averaged SPW amplitudes $A_{\sigma s}$ and negative phases $-\alpha_{\sigma s}$ (referred to as phases hereafter) are shown in Figs. 4 and 5 for wave 1 or mode (0, 1) and wave 2 or mode (0, 2) of December–January and in Figs. 6 and 7 for those of March–April. The standard deviations for the mean amplitude and phase are roughly 2 m s^{-1} and 10° below 100 km and increase to 6 m s^{-1} and 30° above 110 km. Larger errors of phase estimates occur at heights where the amplitude is small. Thus, the phases are displayed only for the regions with amplitudes greater than 5 and 3 m s^{-1} for the zonal and meridional components, respectively. The regions of latitudes 60° and 70° in both hemispheres, where the wave amplitudes are generally smaller than the threshold values, are not shown. The phase lines are labeled with the longitude of maximum eastward or northward velocities of each wave mode (restricted to 0°–180° for wave 2). There are latitude–altitude regions where the phases change rapidly so that a phase jump occurs. The phase jump lines are referred to as nodal phase lines, which separate or localize the SPW fields in the MLT heights into the regions with different amplitudes and phases. For better presentation, the zero phase lines are also used to represent the nodal phase jump lines, which are not labeled due to the high phase gradients.

In Figs. 8 and 9, we display longitude–latitude presentations of the SPW fields at 96 km, where the zonal and meridional perturbation velocities generally attain their maximum magnitudes. The wind fields are synthesized by using amplitudes and phases of both wave modes. Most features apparent in these two figures are common between 90 and 99 km.

a. Mean zonal winds and localization of SPW fields

The propagation of SPW is sensitive to mean zonal wind structure (Schoeberl and Geller 1977). As seen in Fig. 3, the mean zonal wind fields for December–January and March–April are similar to those reported by Wang et al. (1997) in their empirical horizontal wind model based on WINDII green line measurements of 1992–93 and are in agreement with HRDI observations (Lieberman et al. 1993; Burrage et al. 1996). The sol-

→

FIG. 1. Aliasing map of wave 1 (upper panels) and wave 2 (lower panels) under WINDII sampling at 50°S (left panels) latitude and the equator (right panels) during March and April 1992. The spectral power leakage of the input artificial signals into other components are expressed by the percentage of aliasing and contoured using a 20% interval. The most serious aliases are nonmigrating diurnal tides (1, 0) and (1, 2) for wave 1 or (0, 1), and (1, −1) and (1, 3) for wave 2 or (0, 2). The aliasing magnitudes are 50% at 50°S and less than 20% at the equator. For the latter case, the nonmigrating, diurnal and semidiurnal tidal components are not shown in the contours due to their small magnitude of less than 20%.

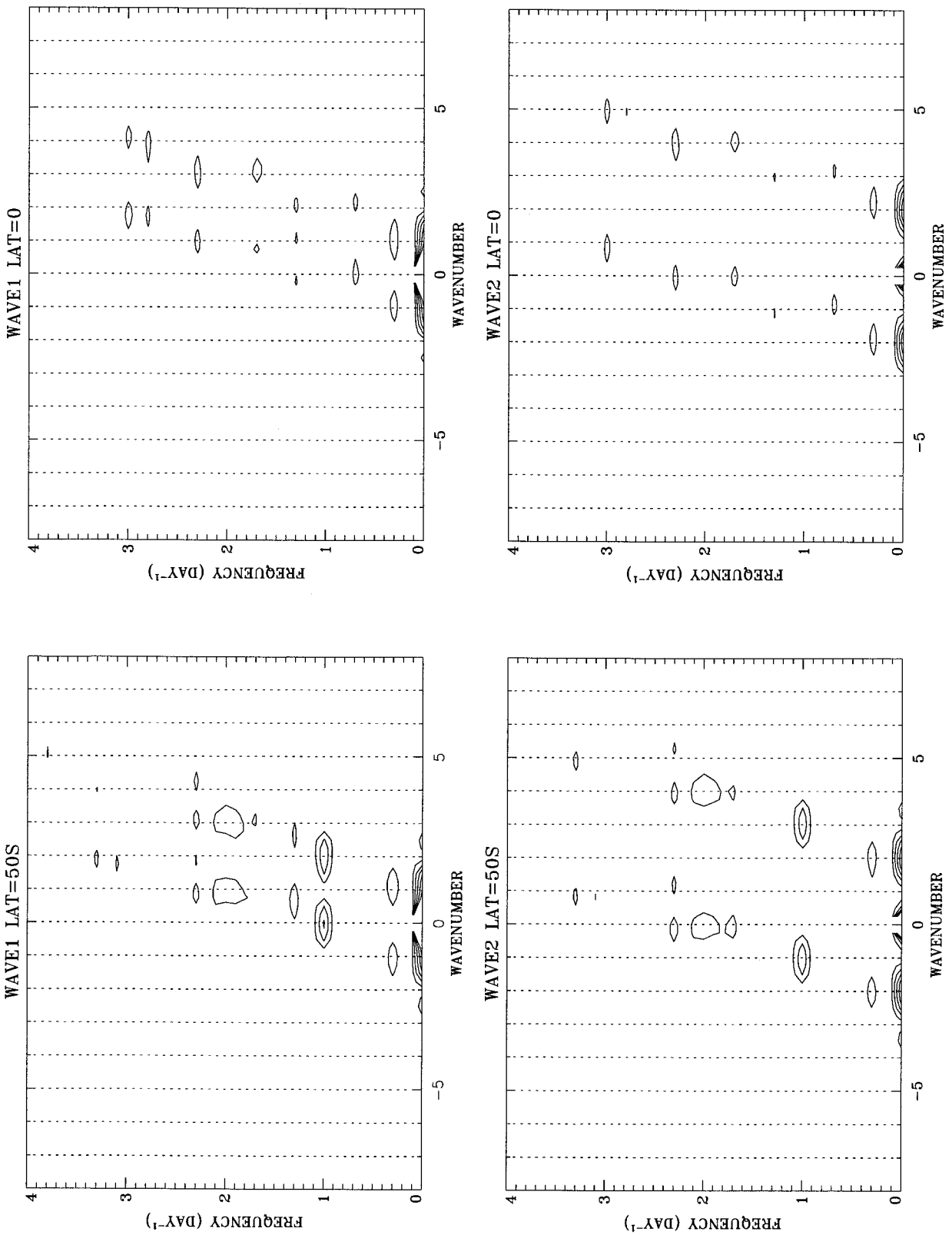

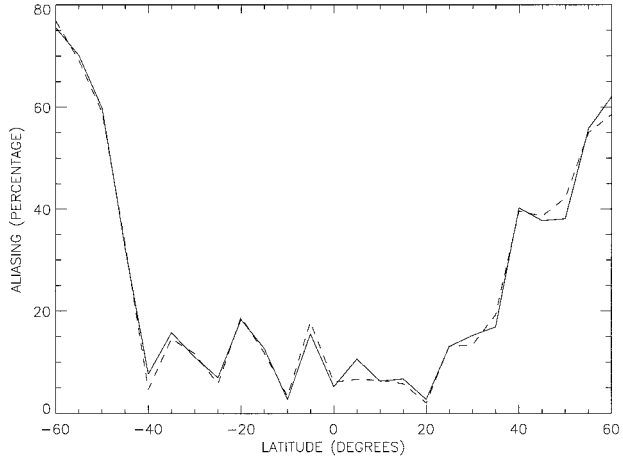

FIG. 2. Latitudinal variations of the aliasing due to the asynoptic WINDII sampling during March and April 1992. Percentages of aliasing are shown for nonmigrating, diurnal tide (1, 2) leaked into wave 1 (solid line) and (1, −1) leaked into wave 2 (dashed line).

stitial mean winds at low latitudes around the equator are dominated by westward winds of −10 to −30 m s^{-1} between 90 and 120 km, with interannual variability less than 10 m s^{-1} in amplitude. The equinoctial zonal winds at the low latitudes show large interannual variations and are dominated by stronger westward winds below 105 km and weaker eastward winds above 105 km, with maximum westward winds of 80 m s^{-1} around 93 km and peak eastward winds of 30 m s^{-1} at 110 km. At midlatitudes centered near 40°, eastward and westward jets are found to have speeds of 10–50 m s^{-1}, with stronger eastward winds around 96 km in the summer and westward winds above 110 km in the winter. Relatively strong semiannual variations are exhibited at the midlatitudes, particularly in the Northern Hemisphere, resulting in the weaker equinoctial winds or wind reversals in comparison with corresponding solstitial winds. For the midlatitude winds of both seasons, the interannual variations are about 10–20 m s^{-1} in amplitude.

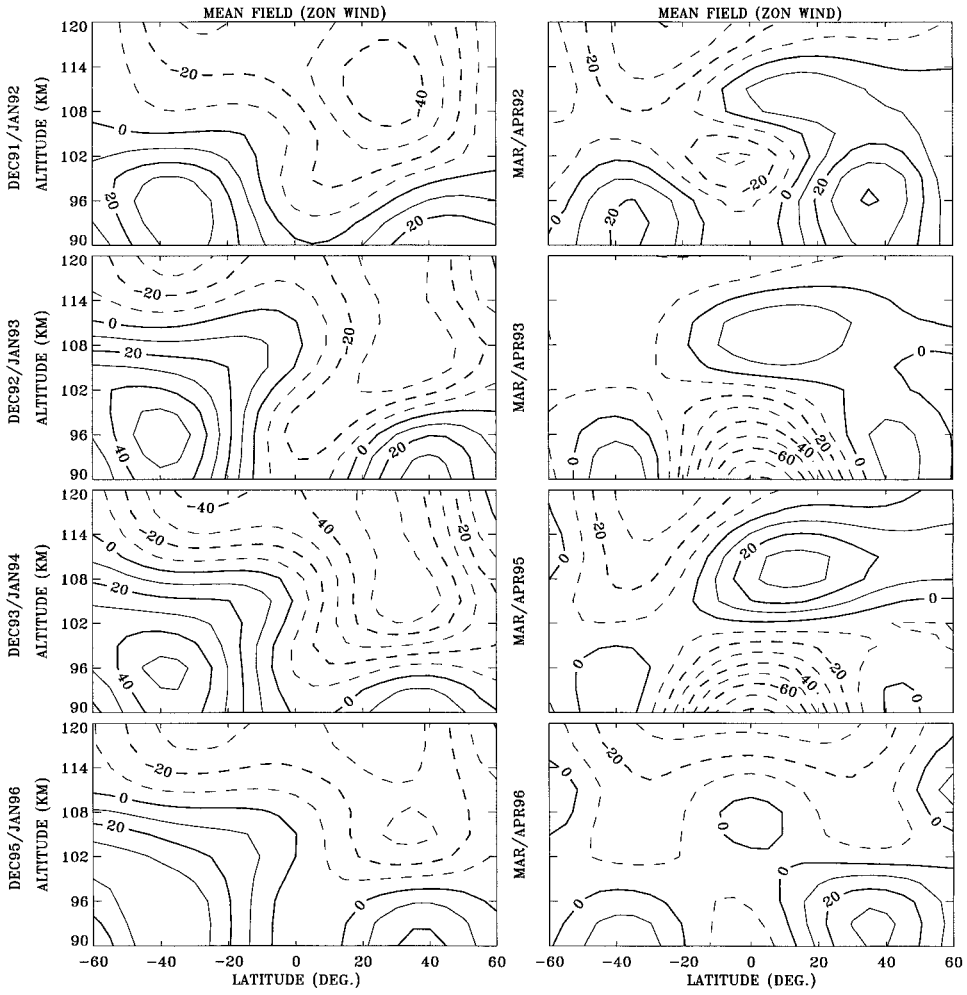

FIG. 3. Zonally averaged zonal wind (m s^{-1}) for two-month periods of December–January (left panels) and March–April (right panels). Westward winds are negative.

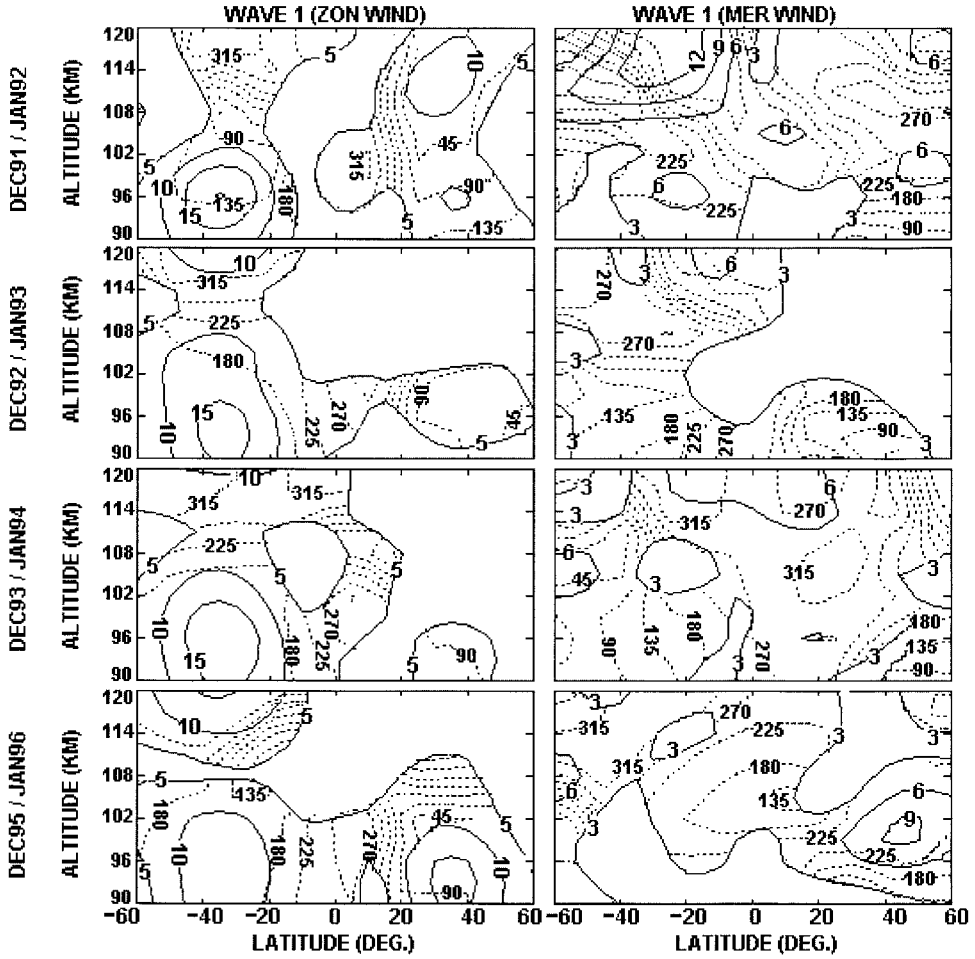

FIG. 4. Meridional contours of amplitude (m s^{-1}, solid line) and negative phase (deg eastward, dotted line) for stationary wave of zonal wavenumber 1 during December–January. The zonal and meridional amplitudes are contoured by 5 and 3 m s^{-1} intervals, respectively. The phases are contoured using a 45° interval and displayed only for zonal and meridional amplitudes greater than 5 and 3 m s^{-1}, respectively.

The above-described zonal mean winds in the MLT region are different from those in the stratosphere and mesosphere. It is well known that the zonal circulation in the low atmosphere is strong during solistice seasons, with westward winds in the summer hemisphere and eastward winds in the winter hemisphere. The equinoctial circulations are relatively weak, with a rather strong wind reversal in both hemispheres in springtime. For each season and each hemisphere, however, the wind directions remain unchanged in the region between ~20 and 90 km. Maximum velocities in both hemispheres for the two seasons generally occur in the midlatitude mesosphere. Above the maxima, the stratospheric/mesospheric jets decrease in amplitude with increasing height and reverse near the mesopause. This height region is close to the lower border of our WINDII observations.

In response to the MLT background wind structures with large meridional and vertical gradients, the SPW fields observed by WINDII are strongly localized. In regions of zero mean zonal wind, SPWs with zero zonal phase speed are subject to critical layer effects. The waves are absorbed, reflected, and refracted at or near these regions (Killworth and McIntyre 1985) and cannot propagate across them. Near the regions, the wave phases change rapidly and the nodal phase jump lines are presented. The solstitial wave-1 variations (Fig. 4) exhibit large hemispheric asymmetry in amplitude. The latitudinal localization is characterized by the nodal phase jump lines, which are generally shifted northward from the equator by 10°–20° and 20°–30° for the zonal and meridional components, respectively. Similar shifts of the nodal phase lines are also presented in radiance measurements in the upper mesosphere by satellites (e.g., Fig. 5.4 of Andrews et al. 1987). There, the geopotential phase lines of wave 1 incline to merge together around 40°N approximately at 90 km, with a tendency toward the equator by 10° at higher levels. This is thought to be controlled by the background temperature gradients in the hot winter and cold summer mesopause

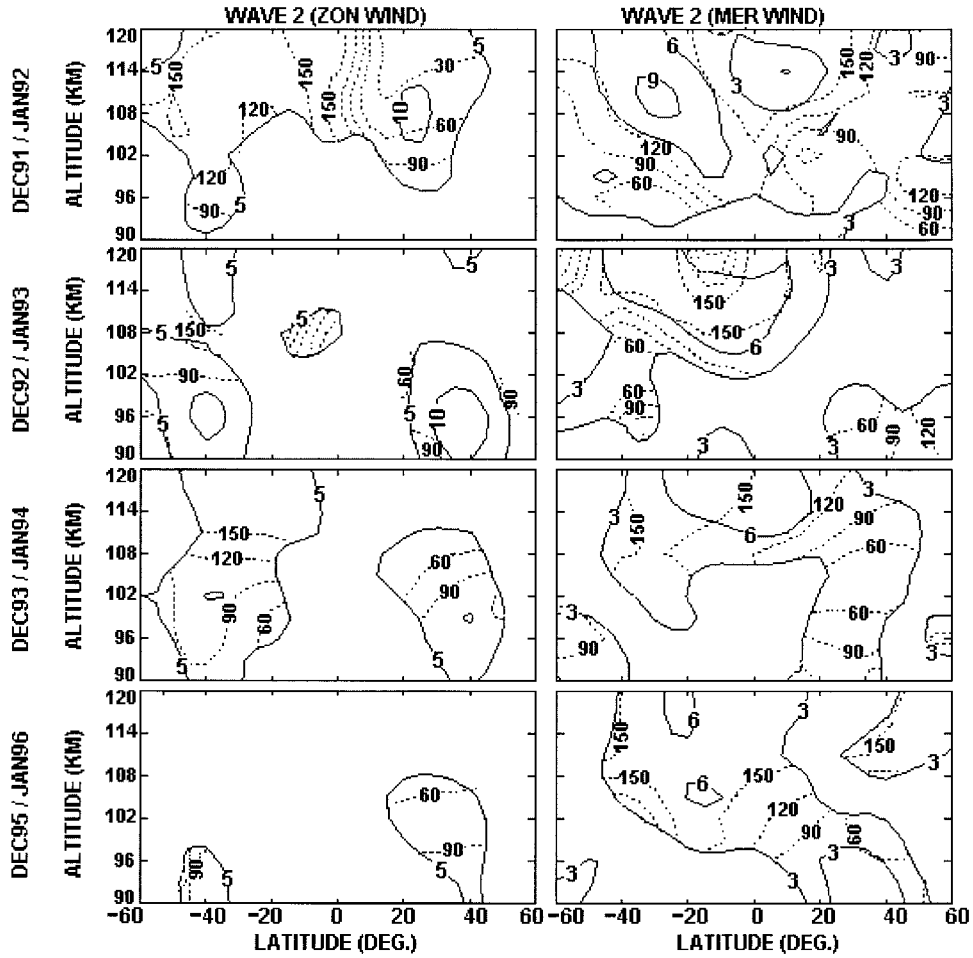

FIG. 5. Same as Fig. 4 but for zonal wavenumber 2. Also, the phases are contoured using a 30° interval.

regions. For the solstitial wave-2 variations of WINDII winds (Fig. 5), the wave amplitudes tend to be symmetric about the equator. A similar feature is observed for both SPW modes at equinox (see Figs. 6 and 7). This is likely associated with the critical layer effects of the zero mean zonal winds, which are fairly symmetric about the equator in spite of the hemispheric asymmetry in the mean wind amplitude (Fig. 3). Near the critical layer's upper heights, the wave amplitudes do not go to zero but show amplitude minima, probably due to complex dynamics such as interference between propagating and reflected waves in the critical regions.

b. Solstitial SPW fields

The observed solstitial SPW fields (Figs. 4, 5, and 8) are dominated by wave-1 variations and have a local summer maximum in zonal component. For both wave modes, maximum zonal amplitudes of 5–20 m s^{-1} generally occur in the regions of maximum (positive or negative) mean zonal winds around 35° latitude in both hemispheres. The summer maxima of wave 1 (Fig. 4) have significantly large amplitudes of 15–20 m s^{-1}, primarily peaked at 96 km around 120°–135°E. The wave perturbations extend over a wide latitude–height region, and secondary maxima are seen at 115–120 km around 315°E. The wave penetration across the equator is also apparent at 97–100 km, with amplitudes of 5 m s^{-1} and phases around 300°E. In contrast, the winter maxima of wave 1 are much weaker and more localized and show hemispheric differences of 10 m s^{-1} and ±30° in amplitude and phase, respectively. The wave-2 variations (Fig. 5) are relatively weak, with amplitudes of 5–10 m s^{-1} and phases around 90°–120°E, and exhibit considerable hemispheric symmetry. The features observed in the winter hemisphere are largely consistent with those reported in S97 for HRDI measurements in December 1992–94.

Both summer and winter maxima of the zonal components in our observations have relatively stable latitude and height locations during the four years but show year-to-year amplitude differences and phase shifts of 10 m s^{-1} and ±30°. Larger interannual variabilities are observed in the winter hemisphere and for wave 2. In

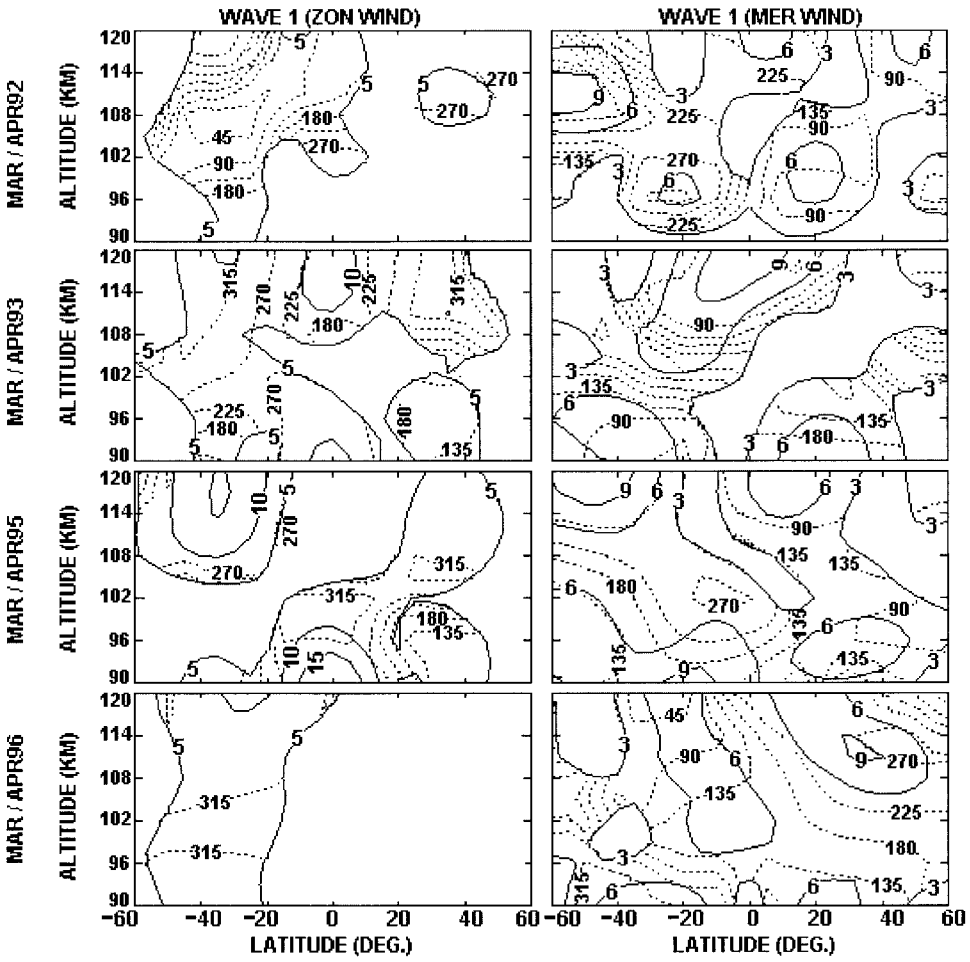

FIG. 6. Same as Fig. 4 but for March–April.

particular, the contributions of wave 2 become significant in the Northern Hemisphere in December 1992–January 1993 and December 1993–January 1994 so that a wave-2 pattern is evident in the total wave perturbation winds (Fig. 8). This is in agreement with the HRDI measurements presented in S96. The 1992 HRDI data at latitudes 40°–60°N and altitudes 75–81 km in February are characterized by a wave-1 pattern. The largest zonal velocities are centered in the region 120°–240°E with southward winds at 100°E. However, the 1994 HRDI SPW field is dominated by wave-2 variation, with two regions of southward winds (around 100°E and 250°–350°E) and weaker eastward winds at higher latitudes of the coverage.

The WINDII-observed solstitial SPW variations of the meridional component exhibit larger geographic and interannual variabilities in amplitude and phase. As seen in Figs. 4, 5, and 8, there is a tendency for zonal and meridional maximum amplitudes to be partially in phase and for maxima in zonal wind to occur to the west of maxima in meridional wind, with a phase difference of 30° or as large as 90°. Away from the amplitude maxima, the phase relations are more complicated. At low altitudes below 105 km, both wave modes achieve meridional amplitude maxima of 3–6 m s^{-1} around latitudes 30°–40° and altitudes 96–105 km. Their longitudinal phases are between 135° and 225°E for wave 1 and between 60° and 90°E for wave 2. In comparison, the HRDI measurements for December of 1992–94 have reported meridional wave-1 maxima of 4–8 m s^{-1} around 300°E between 90 and 100 km at 40°N, with the largest and smallest amplitudes corresponding to 1992 and 1994, respectively. As shown in Figs. 4 and 5 for WINDII observations, at higher levels around and above 105–110 km, both modes show larger amplitudes extending to low latitudes and phases located between 225° and 360°E for wave 1 and between 120° and 150°E for wave 2.

We more closely examine the meridional phases, whose vertical and meridional gradients are associated with EP flux. In our observations, different features of the wave propagations are seen in the latitude regions divided by the above-mentioned nodal phase jump lines around 10°–30°N. At low altitudes below 105 km, the

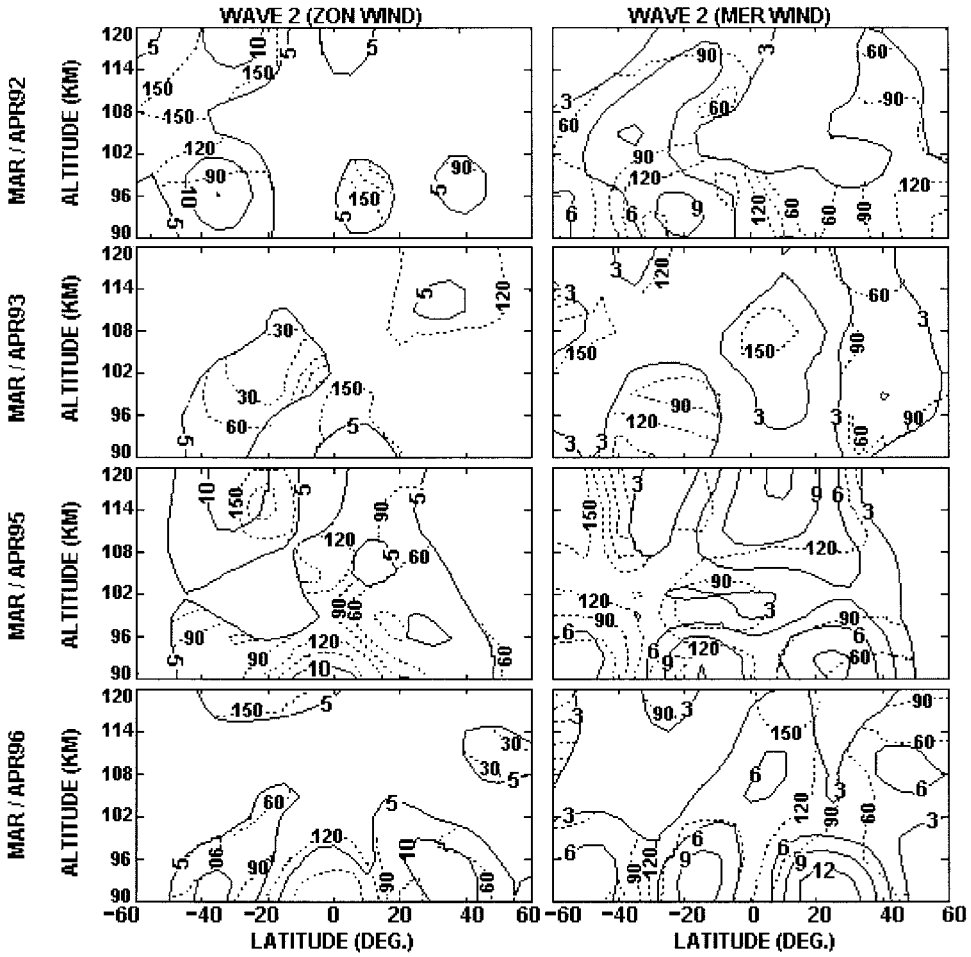

FIG. 7. Same as Fig. 5, but for March–April.

phases of both modes in the southern latitude interval (Figs. 4 and 5) progress predominantly westward with decreasing latitude, implying EP fluxes propagating from the winter latitudes into the summer hemisphere with penetration across the equator. The phases generally tilt westward with increasing height, representing upward EP fluxes. In the northern latitude interval, however, the meridional phases of both modes at the lower heights generally progress eastward with decreasing latitude, implying poleward EP fluxes. The wave-1 phase lines are seen to tilt eastward with increasing height, indicating downward EP fluxes, while the wave-2 phases tend to be vertical, suggesting evanescence. These features are different from those of SPW in the stratosphere, but quite consistent with those inferred from satellite radiance measurements in the upper mesosphere. As shown in Fig. 5.4 of Andrews et al. (1987), the geopotential wave-1 phase between 50° and 70°N at 90-km level is 180°E and appears to tilt eastward with increasing height and latitude. The geopotential wave-2 phase is nearly vertical, with poleward EP flux. Similar eastward phase tilt with height is also presented between 90 and 100 km in the HRDI data of 1993, while the nodal phase jump lines are shown at 90 km for 1992 and at 100 km for 1994. Finally, we note that the wave modes observed by WINDII at higher levels in both hemispheres are predominantly vertically evanescent, as shown by nearly vertical phase lines, with a tendency of downward-equatorward EP flux for wave 1 and poleward for wave 2. Geomagnetic processes are thought to be a controlling factor in producing the trapped disturbances (Volland 1979).

The observed features of the winter SPW field are believed to be primarily associated with an in situ generation of the planetary waves due to longitudinally asymmetric gravity wave drag (e.g., S96; S97; McLandress and McFarlane 1993; McLandress and Ward 1994). The gravity waves generated in the troposphere during a variety of meteorological and orographic situations can have zonal asymmetries resulting from the distribution of orographic features and the flows in the troposphere. The upward propagating gravity waves are filtered by the stratospheric flows, which are zonally asymmetric due to the existence of stratospheric plan-

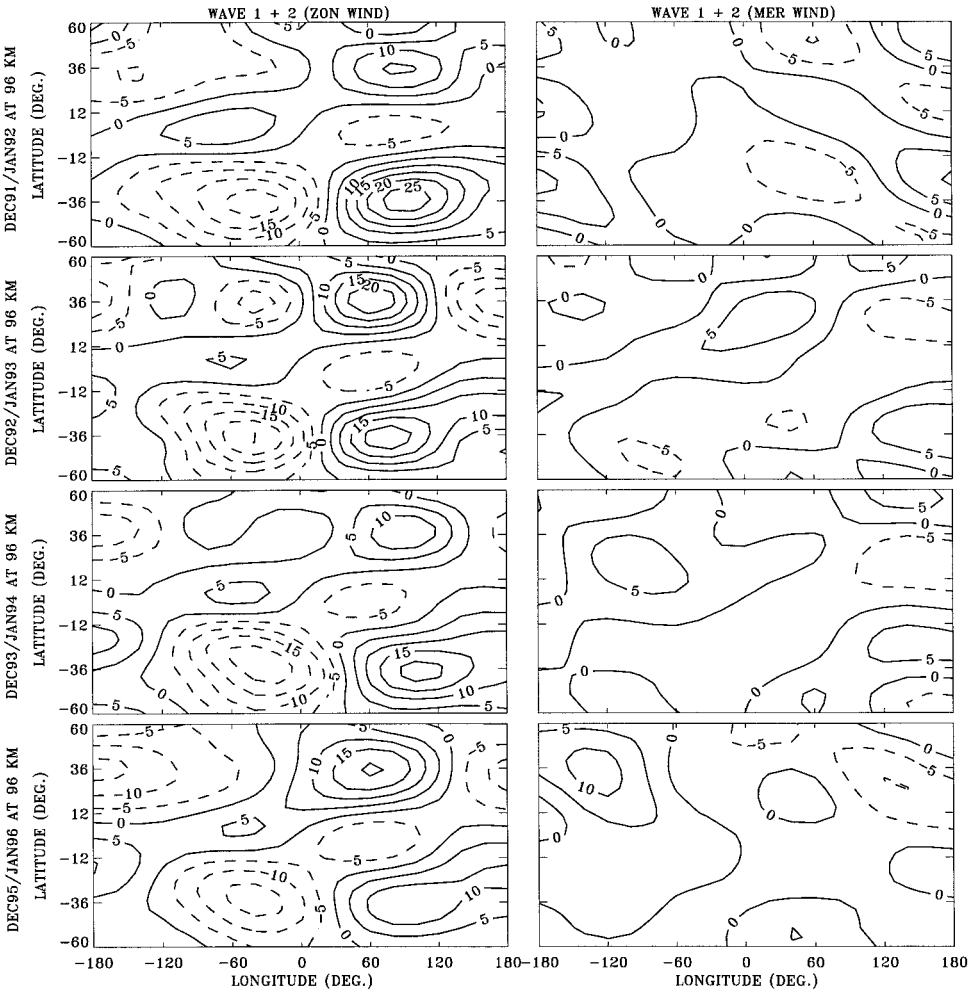

FIG. 8. Longitude–latitude presentation of the synthesized stationary wave fields of zonal wavenumber 1 and 2 at 96 km during the two-month period of December–January. The winds in meters per second are contoured using a 5 m s^{-1} interval. Westward and southward winds are negative.

etary waves. The filtering will also give rise to zonal asymmetries in the ability of gravity waves to penetrate into the mesosphere. The gravity waves that penetrate into the mesosphere during winter tend to be those that are stationary or have westward phase speeds, which are less likely to encounter a critical level in the winter stratospheric eastward flows. When these upgoing gravity waves dissipate or break in the mesosphere, the wave drag forcing will have planetary-scale zonal asymmetries and can damp (for gravity wave phase speeds near stationary) or enhance (for fast-moving gravity waves) the planetary-scale winds. The pattern change from wave 1 to wave 2 in the observed winter SPW fields, as mentioned previously, may suggest variability of the wave drag in time and space. In addition to the in situ excitation, continuous propagation of SPW from the lower stratosphere–mesosphere to MLT heights may also play a role in the observed SPW components, particularly for early winter observations.

Our observations have also revealed the presence of a local summer maximum of 10–25 m s^{-1} in the zonal SPW field. Its excitation mechanism, however, is not fully understood at the moment. It is well known that the planetary waves excited at lower altitudes typically cannot propagate into the summer MLT region due to the attenuation by stratospheric westward winds. Thus, the summer maximum is most unlikely to be associated with any continuous propagation or leakage of upgoing SPW motions. As referred to in the above discussions about the winter SPW field, in situ forcing of azonal gravity wave drag could be largely responsible for generation of the summer maxima. Gravity waves with a broad spectrum of phase speeds can propagate upward into the summer MLT region. Since upward propagation of orographic gravity waves with phase speed near zero is inhibited by the mean flow structures in the low atmosphere (Holton 1983), we may expect that the waves having fast-moving phase speeds and emanating from

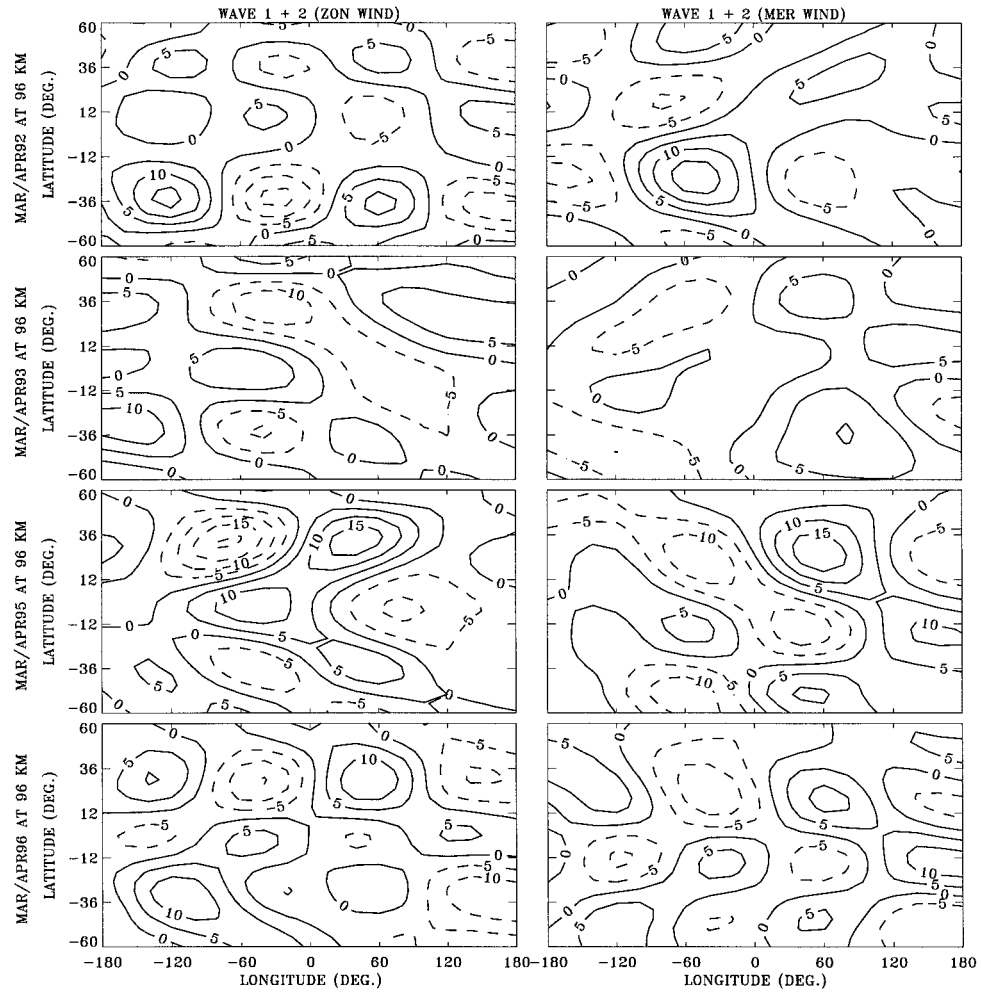

FIG. 9. Same as Fig. 8 but for March–April.

sources other than topographic variations are of considerable importance. Due to the filtering of longitudinally varying flows in the low atmosphere, the upgoing gravity waves must propagate azonally and predominantly eastward in the southern latitudes and westward in the northern regions as well as break at the lower and higher altitudes of strong eastward and westward mean flows, respectively, where the critical levels are encountered. The breaking of fast-moving gravity waves will enhance the planetary-scale winds. More investigation in this direction is required and will certainly provide a better understanding about the wave dynamics in the MLT region.

c. Equinoctial SPW fields

As shown in Figs. 6, 7, and 9, the observed equinoctial SPW fields are characterized by wave-2 variations. The wave amplitude maxima of both modes generally occur between 90 and 100 km around 35° latitude in both hemispheres and are nearly symmetric about the equator. The wave amplitudes are large in March–April 1992 in comparison with those in 1993, consistent with HRDI results shown in S96. The waves are also seen to propagate in wide latitude–altitude regions and across the equator at 110-km level, where weaker eastward flows exist. In comparison with the solstitial fields at the lower altitudes, the zonal amplitudes significantly decrease for wave 1 (Figs. 4 and 6) but remain nearly the same for wave 2 (Figs. 5 and 7), and the meridional amplitudes generally increase, particularly for wave 2, reaching maxima of 6–12 m s^{-1}. These seasonal variations result in the dominance of wave-2 perturbations over the equinoctial SPW fields. Since deeper penetration of SPW into the MLT region is expected during the equinoctial periods, the decrease of zonal amplitudes may suggest a significant reduction of in situ forcing, which is in agreement with minima in gravity wave intensities observed at Saskatoon and Adelaide at times around the spring and fall reversals in zonal mean circulation (Vincent 1990).

The phases of the zonal components at the lower al-

titudes show eastward velocity maxima around 60° and 240°E and westward maxima around 150° and 330°E. The meridional phases indicate Eliassen–Palm (EP) fluxes southward in 1992 and equatorward in 1996 for both modes and poleward for wave 1 and equatorward for wave 2 in 1993 and 1995, with vertical propagations or evanescence. At the higher altitudes where westward winds are dominant, the waves become evanescent, showing larger hemispheric asymmetry in amplitude and a tendency of downward equatorward EP flux. The geographic and interannual variabilities observed in the meridional phases, significantly larger in March–April than those in December–January, imply the irregular EP flux divergences and are consistent with the statistics of SPW in the mesosphere using the climatological radiance data of Marks (1989). This may reflect variations of the relative importance between in situ forcings and continuous propagations of SPW.

4. Concluding remarks

Based on WINDII wind observations in 1991–96, we have obtained a climatology of SPW between 90 and 120 km. The most interesting result is the persistent stationary wave-1 maximum in summer. The characteristics of the longitudinal variations are summarized as follows.

1) The solstitial fields below 105 km are dominated by wave 1 and characterized by a summer maximum at 35° latitude around 96 km, with eastward velocity maxima of 10–25 m s^{-1} and phases around 90°E. The waves can penetrate across the equator and into the winter hemisphere to 10°–30° latitude. The meridional amplitudes are 5–15 m s^{-1}. The phases indicate EP flux downward and poleward in the poleward winter latitudes and vertically varying and toward the summer pole in the equatorial winter and summer region. The hemispheric amplitude and phase differences are 10 m s^{-1} and 30°, respectively.
2) For equinoctial fields, wave-2 variation prevails at the lower altitudes and extends over wide latitude–height regions, with considerable symmetry about the equator. The amplitudes of wave 1 are significantly smaller in comparison with those of the solstitial periods. The eastward wind maxima are centered at midlatitudes and at longitudes near 60° and 240°E. The meridional amplitudes and phases display more geographic and temporal variabilities, implying more irregular EP fluxes.
3) Throughout the year, wave penetrations across the equator are observed, with zonal maxima of 5–10 m s^{-1} at 97–100 km in December–January and 110 km in March–April.
4) Interannual variations are 10 m s^{-1} in amplitude and 30° or more in phase. For individual wave modes, the zonal wind variation is strongly geographically fixed in all four years, with maxima and minima appearing at similar locations. The meridional component is more variable, although some features occur in the same area during all years. However, in the winter hemisphere, relative importance of the two modes may significantly change, especially during 1993–95, when the wave-2 amplitudes dominated the winter SPW fields.
5) At the upper heights above 105 km, where strong westward mean winds are dominant, the waves are predominantly evanescent, as shown by the phase jump lines or nearly vertical phase lines.

The observed features at altitudes below 105 km in the winter hemisphere are consistent with those obtained from satellite radiance and HRDI wind measurements in the upper mesosphere. The existence of a local summer maximum is well established, but its origin is not fully understood. In situ forcing due to azonal gravity wave drag is thought to be the primary factor responsible for it. Such wave drag can be induced by orography and by filtering processes due to longitudinally varying planetary/tidal waves. Fast-moving gravity waves emanating from sources other than topographic variations may play an important role. More studies are required to better understand these relationships.

Acknowledgments. The WINDII project was jointly sponsored by the Canadian Space Agency and the Centre National d'Etudes Spatiale. The Centre for Research in Earth and Space Technology is a designated Center of Excellence supported by the Province of Ontario's Technology Fund. We also acknowledge many important and helpful discussions from I. C. McDade, A. S. Medvedev, and A. I. Pogoreltsev regarding the present manuscript and assistance from C. Climie in data processing.

REFERENCES

Andrews, D. G., J. R. Holton, and C. B. Leovy, 1987: *Middle Atmosphere Dynamics.* Academic Press, 226–235.

Barnett, J. J., and K. Labitzke, 1990: Climatological distribution of planetary waves in the middle atmosphere. *Adv. Space Res.,* **10,** 63–91.

Burrage, M. D., and Coauthors, 1996: Validation of mesosphere and lower thermosphere winds from the high resolution Doppler imager on *UARS. J. Geophys. Res.,* **101,** 10 365–10 392.

Hedin, A. E., and Coauthors, 1996: Empirical wind model for the middle and lower atmosphere. *J. Atmos. Terr. Phys.,* **58,** 1421–1447.

Holton, J. R., 1983: The influence of gravity wave breaking on the general circulation of the middle atmosphere. *J. Atmos. Sci.,* **40,** 2497–2507.

Killworth, P. D., and M. E. McIntyre, 1985: Do Rossby-wave critical layers absorb, reflect or over-reflect? *J. Fluid Mech.,* **161,** 449–492.

Lieberman, R. S., and Coauthors, 1993: Zonal mean winds in the equatorial mesosphere and lower thermosphere observed by the high resolution Doppler imager. *Geophys. Res. Lett.,* **20,** 2849–2852.

Marks, C. J., 1989: Some features of the climatology of the middle atmosphere revealed by *Nimbus 5* and *6. J. Atmos. Sci.,* **46,** 2485–2508.

McLandress, C., and N. A. McFarlane, 1993: Interactions between orographic gravity wave drag and forced stationary planetary waves in the winter Northern Hemisphere middle atmosphere. *J. Atmos. Sci.,* **50,** 1966–1990.

——, and W. E. Ward, 1994: Tidal/gravity wave interactions and their influence on the large-scale dynamics of the middle atmosphere: Model results. *J. Geophys. Res.,* **99,** 8139–8155.

Medvedev, A. S., A. I. Pogoreltsev, and S. A. Sukhanova, 1991: Simulation of the global structure of stationary planetary waves. I. Penetration across the equator. *Izv. Akad. Nauk U.S.S.R., Atmos. Oceanic Phys.,* **27,** 813–824.

Pogoreltsev, A. I., 1996: Simulation of the influence of stationary waves on the zonally averaged circulation of the mesosphere/lower thermosphere region. *J. Atmos. Terr. Phys.,* **58,** 901–909.

——, and S. A. Sukhanova, 1993: Simulation of the global structure of stationary planetary waves in the mesosphere and lower thermosphere. *J. Atmos. Terr. Phys.,* **55,** 33–40.

Salby, M. L., 1982a: Sampling theory for asynoptic satellite observations. Part I: Space–time spectra, resolution, and aliasing. *J. Atmos. Sci.,* **39,** 2577–2600.

——, 1982b: Sampling theory for asynoptic satellite observations. Part II: Fast Fourier synoptic mapping. *J. Atmos. Sci.,* **39,** 2601–2614.

Schoeberl, M. R., and M. A. Geller, 1977: A calculation of the structure of stationary planetary waves in winter. *J. Atmos. Sci.,* **34,** 1235–1255.

Shepherd, G. G., and Coauthors, 1993: WINDII: The wind imaging interferometer on the *Upper Atmosphere Research Satellite. J. Geophys. Res.,* **98,** 10 725–10 750.

Smith, A. K., 1996: Longitudinal variations in mesospheric winds: Evidence for gravity wave filtering by planetary waves. *J. Atmos. Sci.,* **53,** 1156–1173.

——, 1997: Stationary planetary waves in upper mesospheric winds. *J. Atmos. Sci.,* **54,** 2129–2145.

Vincent, R. A., 1990: Planetary and gravity waves in the mesosphere and lower thermosphere. *Adv. Space Res.,* **10,** 93–101.

Volland, H., 1979: Magnetospheric electric fields and currents and their influence on large scale thermospheric circulation and composition. *J. Atmos. Terr. Phys.,* **41,** 853–866.

Wang, D. Y., C. McLandress, E. L. Fleming, W. E. Ward, B. Solheim, and G. G. Shepherd, 1997: Empirical model of 90–120 km horizontal winds from wind-imaging interferometer green line measurements in 1992–1993. *J. Geophys. Res.,* **102,** 6729–6745.

Wu, Dong L., P. B. Hays, and W. R. Skinner, 1995: A least squares method for spectral analysis of space–time series. *J. Atmos. Sci.,* **52,** 3501–3511.